Auxetic solution for enhanced esophageal brachytherapy applicator

Jerome Jean-Joseph, MSc[1], Nikolaus Balagiannis, MD[2], Markus W. Scheppach, MD[3], Selin Temizel, MD[4], Alanna Ebigbo, MD[3], Helmut Messmann, MD[3], Tilman Janzen, PhD[1], Georg Stüben, MD[2]

[1]Medical Physics Department, Augsburg University Hospital, Augsburg, Germany, [2]Radiotherapy Department, Augsburg University Hospital, Augsburg, Germany, [3]Internal Medicine III – Gastroenterology, Augsburg University Hospital, Augsburg, Germany, [4]Department for Hygiene and Environmental Medicine, Augsburg University Hospital, Augsburg, Germany

Abstract

Purpose: In this study, a novel auxetic applicator equipped with four-channel catheters for esophageal brachytherapy was presented.

Material and methods: The applicator, made of a new biocompatible material, has an auxetic helical structure with four channels. Details of applicator modeling, construction, commissioning, and insertion were provided. Initial *ex vivo* trial conducted on a porcine model was outlined.

Results: Simulations and dose calculations closely matched experimental measurements, validating the modeling approach. This applicator achieved highly asymmetric dose distributions. Its unique auxetic helical design allowed smooth insertion, while mitigating sequential inter-fraction hot spot formation.

Conclusions: *Ex vivo* implementation of the applicator demonstrated feasibility, resulting in consistent and reproducible dose distributions. Initial outcomes showed promise for the applicator's efficacy and versatility in intra-luminal or intra-cavitary applications.

Key words: auxetic structure, 3D printing, esophageal applicator.

Purpose

The implementation of medical device regulations (MDR) [1] and good manufacturing practices (GMP) [2] has led to more strict guidelines and controls for custom-made medical devices, including class 2A devices [3], e.g., intra-luminal applicators used in brachytherapy. This new milestone necessitates addressing emerging challenges, such as patient-oriented approaches, sterilization, and cost-effectiveness. This study specifically focused on a multi-channel auxetic structure applicator designed for the treatment of esophageal cancer, aiming to meet these new constraints and challenges. In Germany, where esophageal cancer affects over 7,000 patients annually (2020) [4], it has been established that patients undergoing concurrent brachytherapy (BT) demonstrate a significantly better prognosis compared with those without BT [5].

At our institution, we have been using the Bonvoisin-Gerald esophageal applicator set (B.G. Applicator, Elekta, Sweden) for high-dose-rate brachytherapy treatments of esophageal cancer for around fifteen years. However, due to recent changes in sterilization standards within our hospital, there was an opportunity to explore an alternative solution tailored to patient treatments. Over the years, a wide range of esophageal applicators have been developed, varying from single-use, single-channel boogie applicators, to more complex designs with inflatable components, available in both single- and multi-channel configurations [6, 7].

In this study, a single-use multi-channel applicator with a printed auxetic helical structure was presented, offering adaptability and flexibility.

Material and methods

3D printer

In this study, stereolithography, a type of additive manufacturing technology that employs photo-polymerization to create three-dimensional objects was used. Form 4B (Formlabs Inc., Massachusetts, USA), a professional-grade stereolithography (SLA) 3D printer was utilized due to its high resolution of 0.1 mm and accessibility of biocompatible resins appropriate for the application.

Address for correspondence: Jerome Jean-Joseph, Medical Physics Department, Augsburg University Hospital, Stenglinstraße 2, D-86156 Augsburg, Germany, phone: +49-821400161535,
✉ e-mail: Jerome.jean-joseph@uk-augsburg.de

Mechanical properties	Metric
Ultimate tensile strength	7.2 MPa
Stress at 50% elongation	2.6 MPa
Stress at 100% elongation	4.5 MPa
Elongation at break	135%
Tear strength	22 kN/m
Shore hardness	77-80A
Disinfection compatibility	
Chemical disinfection	70% isopropyl alcohol for 5 minutes

Material

BioMed Flex 80A resin (Formlabs Inc., Massachusetts, USA), a flexible, medical-grade material exhibiting suitable properties for auxetic structures was used (Table 1). This resin, certified under ISO 10993 and USP class VI, is appropriate for applications with short-term mucosal membrane contact (less than 24 hours). However, it is imperative to acknowledge that thermoset polymers, unlike thermoplastics, are non-recyclable [9].

Design of the applicator [10-12]

The applicator shown in Figure 1 features a formable tip designed for smooth insertion into the pharynx. It consist of two flexible, kink-resistant nylon tubes (nylon 6/6, French 6, Zeus, USA), with a shore hardness of D85 arranged in a loop configuration. These biocompatible, USP class VI-approved tubes are approximately 2 meters long in a loop configuration, facilitating access up to the stomach. After radiation testing (50 Gy at 1 cm in a Plexiglas phantom), no significant property changes were observed. Integrated into the applicator design were the following key components: a handle portion with a diameter of French 25, a skeletal structure consisting of 1 mm diameter radiopaque mandrels within each tubular channel, and a helix-shaped corpus.

Corpus (Figure 2)

The primary advantage of a helical structure compared with a straight one for displacement is its ability to undergo torsional deformation without excessive strain. A helical structure can twist and untwist along its axis, allowing greater angular displacement, while minimizing internal stresses and material damage.

Specifically, the helical geometry allows the structure to distribute torsional loads more evenly along its length. As it twists, the helical coils can gradually adjust their pitch and curvature, dissipating the torsional strain over a larger area. In contrast, a straight structure would experience highly localized shear stresses when subjected to torsion, leading to premature failure [13]. The second advantage is the inherent curvature of helical structure that provides increased flexibility and compliance. This enhanced flexibility enables greater linear displacement under bending loads, without exceeding the material's yield strength. Nevertheless, it gives a non-linear motion of the source along the penetration axis of the esophagus, thus reducing the recurrence of the same hot spot locations during successive treatment [13].

The coordinates of dwell source position can be evaluated due to the use of kinematic equation of motion for the helix. The position vector r(t) can be expressed as a function of time t:

$$r(t) = x(t)i + y(t)j + z(t)k$$

where x(t) and y(t) represent any lateral movements of the helix, z(t) is the translational motion along the penetration axis, and i, j, and k are the unit vectors in the x, y, and z directions, respectively.

Assuming a linear function for z(t) representing the translational motion along the penetration axis (z(t) = v.t), where v is the velocity along the penetration axis, and a rotational motion about the helix axis represented

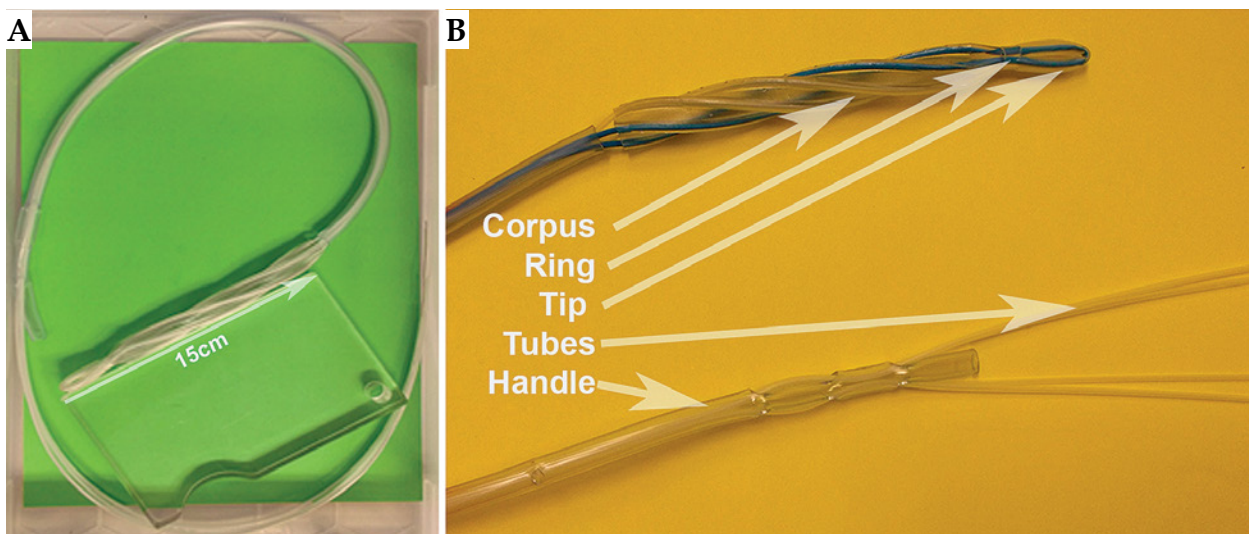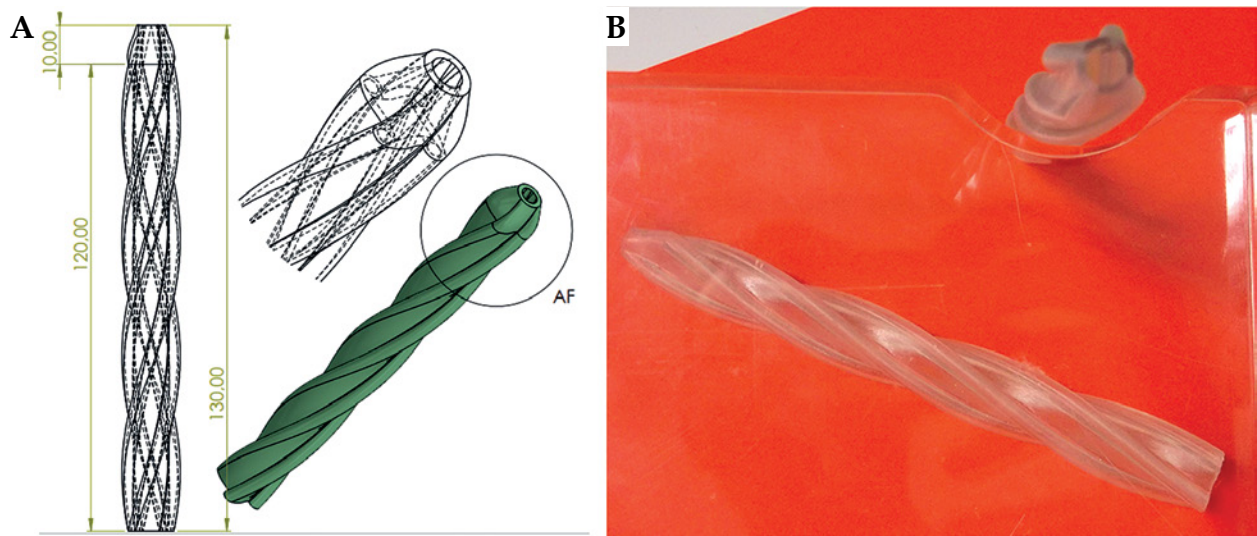**Fig. 1. A**) Applicator overview; **B**) Applicator components

Fig. 2. A) Design rendering of the corpus; **B**) 3D-printed corpus

by an angle $\theta(t) = \omega.t$ (where ω is the angular velocity) can be expressed as:

$$r(t) = (x(t), y(t), v.t)$$

Incorporating the rotational motion:

$$r(t) = (x(t), y(t), v.t) + R(\theta(t))r0$$

Where $R(\theta)$ is the rotation matrix representing the rotation about the helix axis by an angle θ, while $r0$ is the reference position vector of a dwell position on the helix [14].

In this study, an auxetic structure due to its several advantages over non-auxetic (conventional) structures was used. Firstly, auxetic structures exhibit higher shear modulus and resistance to shear deformation as compared with conventional structures. Secondly, when subjected to indentation, auxetic structures undergo lateral expansion instead of contraction, distributing the load more effectively, and increasing resistance to indentation and penetration. Thirdly, an unique deformation mecha-

nism of auxetic structures leads to higher fracture toughness and resistance to crack propagation. Furthermore, auxetic structures can form synclastic (saddle-like) curvatures when bent, unlike conventional structures, which form anticlastic (cylindrical) curvatures. This property is beneficial for adapting to complex shapes, such as the pharynx region [15].

The choice of a tetra chiral auxetic structure (Figure 3) was motivated to provide minimal pressure on the esophageal wall, and assuring enough contact strength to stabilize the corpus. This auxetic behavior can be determined due to negative Poisson's ratio (NPR) under uniaxial tension or compression:

$$\nu = - \frac{-d\varepsilon trans}{d\varepsilon axial} = - \frac{-d\varepsilon y}{d\varepsilon x} = - \frac{-d\varepsilon z}{d\varepsilon x}$$

Where v is the resulting Poisson's ratio, εtrans is transverse strain, εaxial is axial strain, positive strain indicates extension, and negative strain specifies contraction.
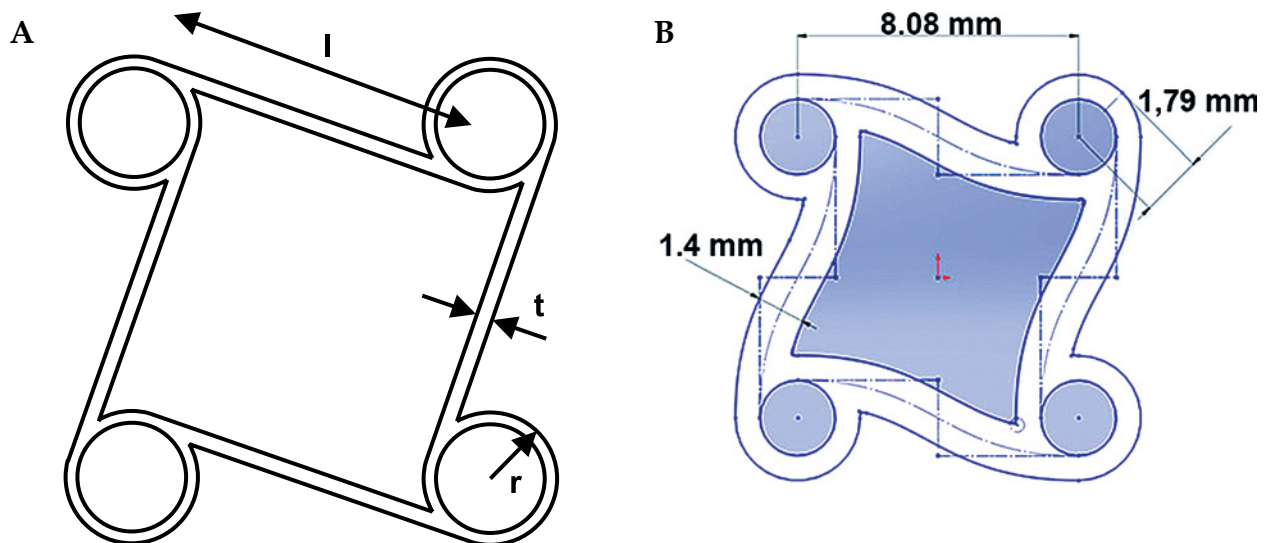

Fig. 3. A) 2D tetra chiral auxetic topology; **B**) 3D cross-section design

In the current modeling approach, the mechanical properties of products made through additive manufacturing (3D printing) techniques were deemed anisotropic. This assumption was based on the findings reported in [16], which demonstrated a directional dependence of the mechanical characteristics for 3D-printed components. Anisotropic nature, in which the properties vary with the loading direction, is a critical factor that must be considered when evaluating the performance and behavior of these components under diverse loading scenarios.

Experimental study and simulations

To gain deeper insights into the anisotropic behavior and its implications, finite element simulations using SOLIDWORKS software package (2023 SP5 Premium, Dassault Systèmes SolidWorks Corporation, Massachusetts, USA) were conducted. By incorporating the dynamic equilibrium equation, the finite element method was utilized to address issues within corpus applicator, providing valuable insights into how the material responds to various forces and stresses over time [17, 18].

Dynamic equilibrium equation

$$\frac{\partial^2 u}{\partial t^2} - \nabla \times (D(\nabla u)\nabla u) = f$$

where u represents the displacement vector field that describes the deformation of the material, t is time, f is any external forces acting on the material, and D is the material's constitutive tensor that describes how stress depends on strain. This tensor is typically non-linear and can depend on the gradient of displacement field.

This equation combines Newton's second law $\frac{\partial^2 u}{\partial t^2}$ with a constitutive relation $\nabla \times (D(\nabla u)\nabla u)$ that accounts for the material's behavior under deformation.

The deformation behavior of the resin material similar to silicone rubber under compressive loading is effectively illustrated by the Mises stress cloud diagram in Figure 4. The von Mises stress, a scalar derived from principal stresses, is widely used to predict the yielding or fracture of ductile materials, such as the resin used in the study.

The figure visually represents the distribution of Mises stress within the model under compressive loading, with warmer colors (e.g., red) indicating higher stress levels, and cooler colors (e.g., blue) denoting lower stress
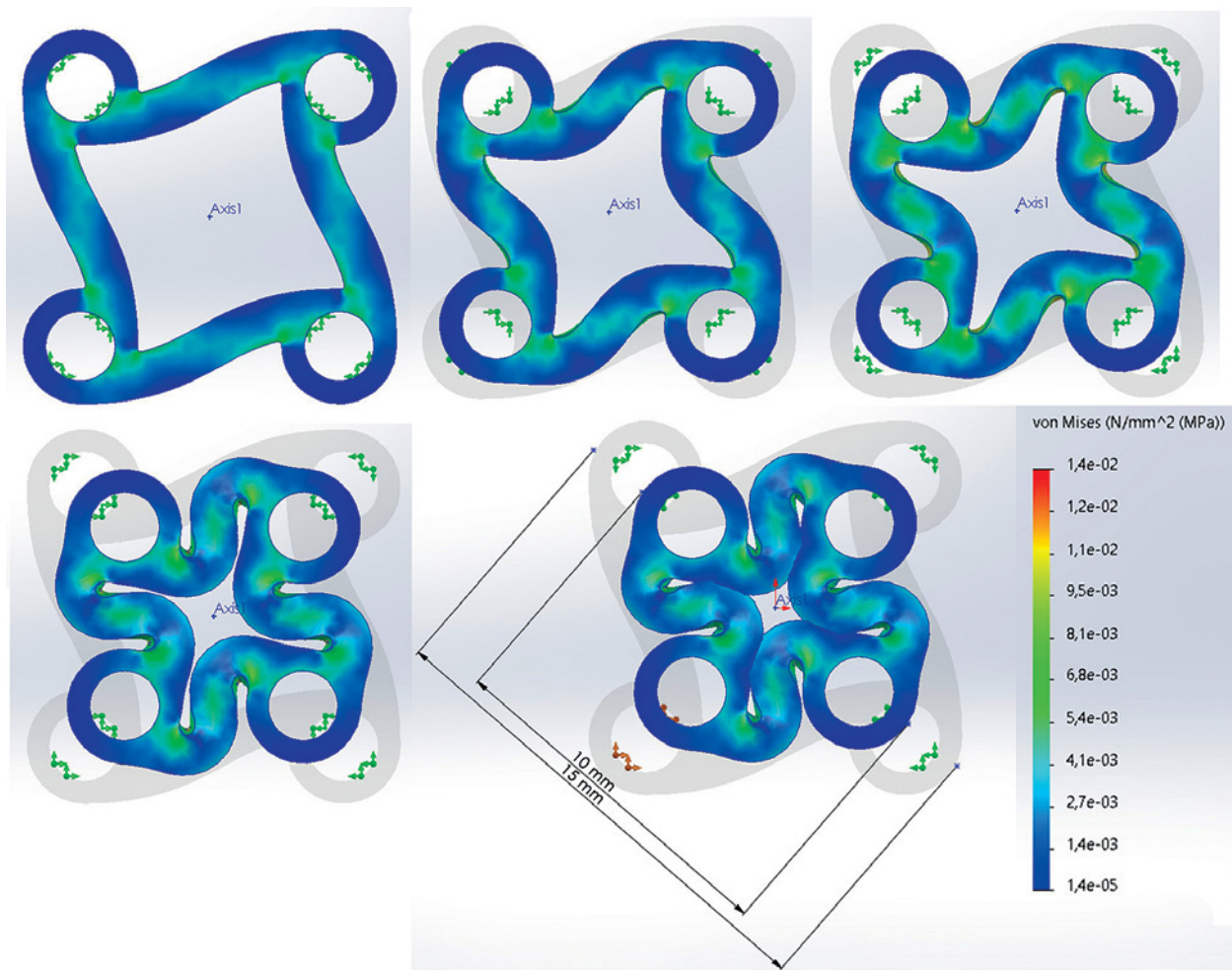

Fig. 4. 2D deformation mode of a 3D tetra chiral structure under compressive convergent forces
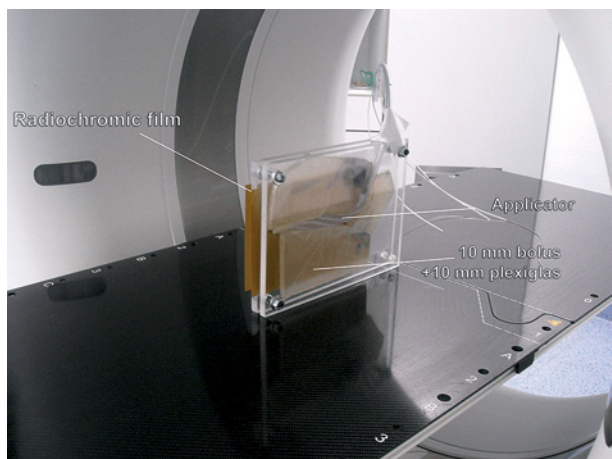
Fig. 5. Applicator in Plexiglas phantom with radiochromic film

levels. By analyzing this figure, we can identify regions where the Mises stress approaches or exceeds the material's yield limit, revealing areas prone to localized deformation or potential failure.

Based on the simulation results and analysis presented, the proposed applicator can be effectively utilized for esophageal diameters starting from 10 mm.

Applicator commissioning

Prior to *ex vivo* utilization, the fully assembled applicator underwent commissioning through a phantom
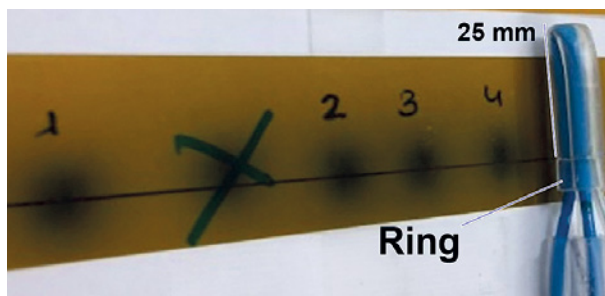

Fig. 6. Tip end irradiation control film

computed tomography study (CT scanner, Siemens SOMATOM Confidence, 2019) (Figure 5). During this assessment, radiochromic film (EBT3, Gafchromic™ Ashland Inc., Wayne, NJ, USA) was employed. Subsequently, autoradiography (Figure 6) of the applicator was conducted to determine the offset (the distance from the visible applicator tips to the first dwell positions) and the appropriate indexer length for HDR afterloader (MicroSelectron, Elekta AB, Stockholm, Sweden).

Upon confirming proper source insertion into the tubes, it was determined that the offset based on the current equipment and configuration was 25 mm, when an indexer length of 952 mm for each channel was selected.

Results

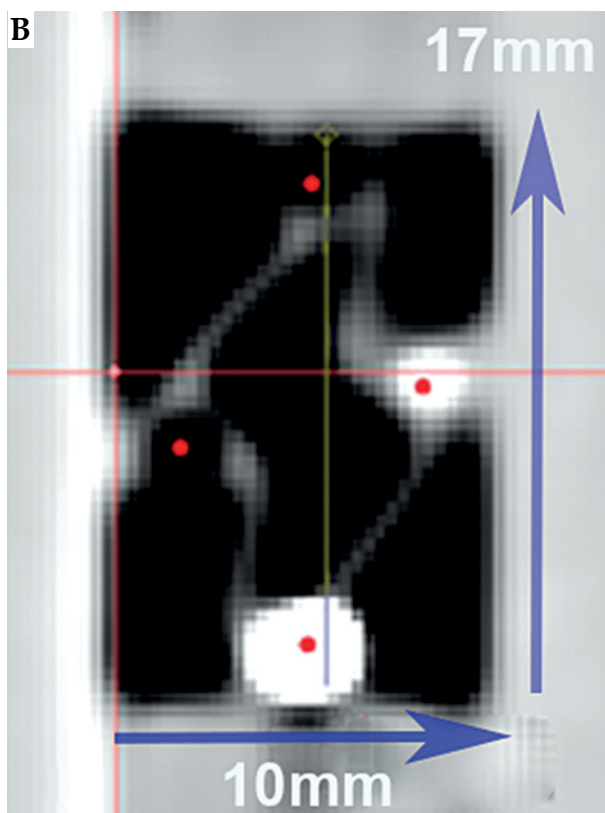Validation of the simulated data through experimental comparison is demonstrated in Figure 7.

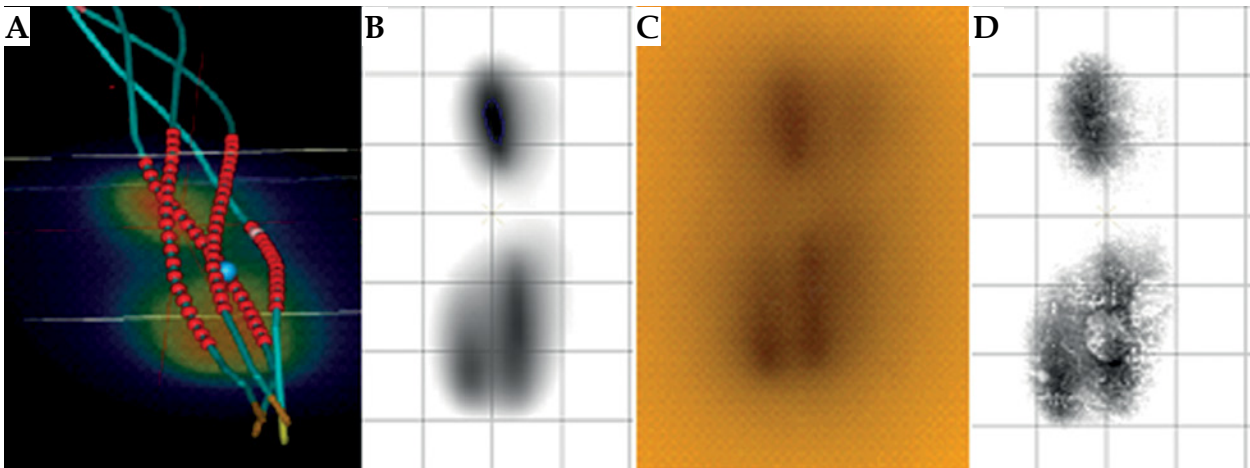**Fig. 7. A**) Contracted corpus; **B**) CT image of expanded corpus

Fig. 8. A) Dose map, **B**) DICOM RT, **C**) radiochromic film, **D**) and scanned film

For dose calculation, Oncentra Brachy® v. 4.6.2 (Elekta AB, Stockholm, Sweden) was utilized. After 72 hours, the films were digitized. Scanning was performed using Epson Perfection V750 Pro scanner (Seiko Epson Corporation, Suwa, Japan), with 96 dpi resolution and 48-bit color depth in black and white light color spectrum (Figure 8). Gamma analysis of the data was carried out using VeriSoft® (PTW, Freiburg GMBH, Freiburg, Germany) package [19, 20]. The results were about 95.6% with 2 mm and 2% criteria, which corresponded to the expectation when man uses TG-43 formalism dose calculations (Figure 9) [21].

Ex vivo model

The study was conducted at the University Hospital Augsburg in collaboration with the Department for Hygiene and Environmental Medicine. A comprehensive protocol was developed to ensure microbiological safety
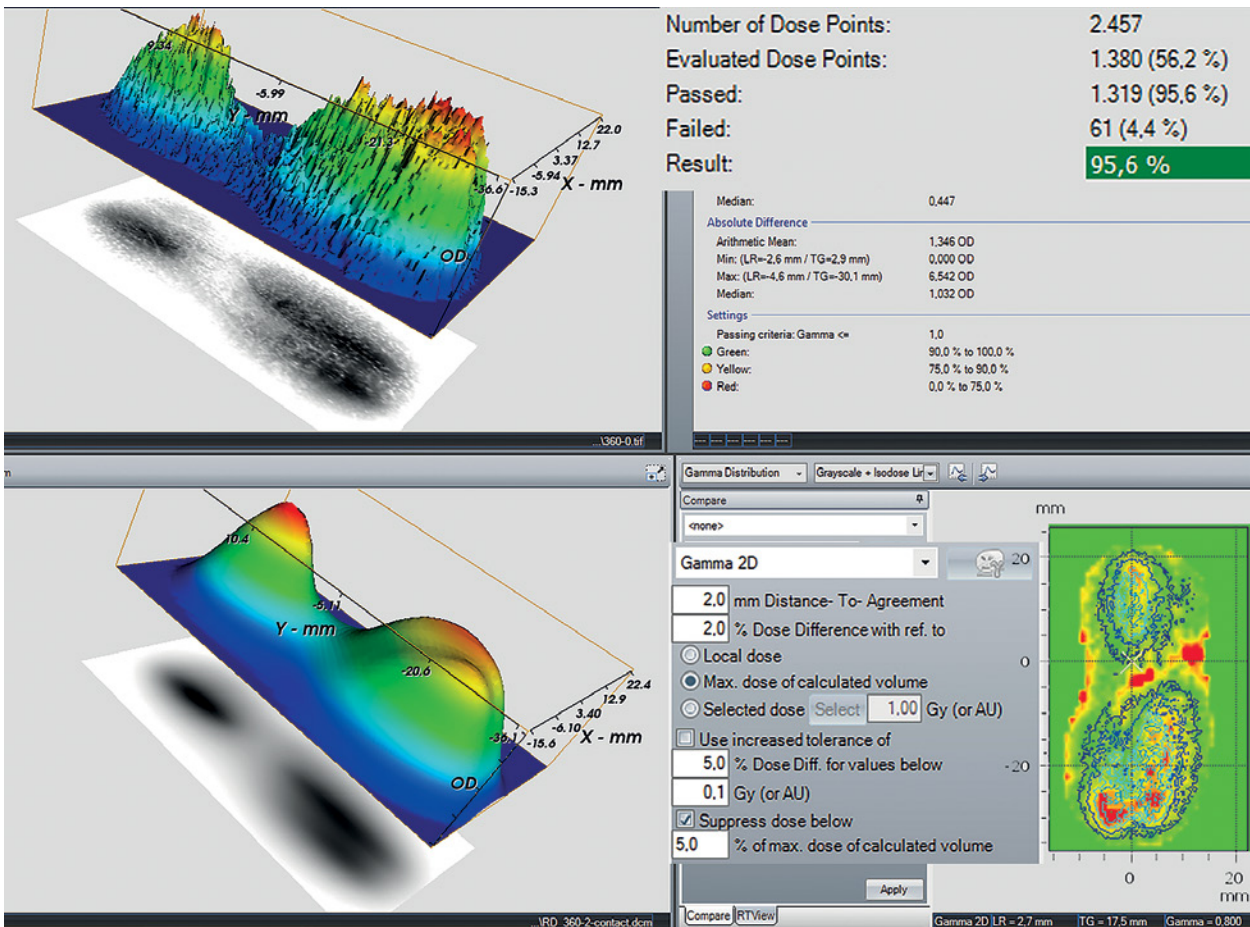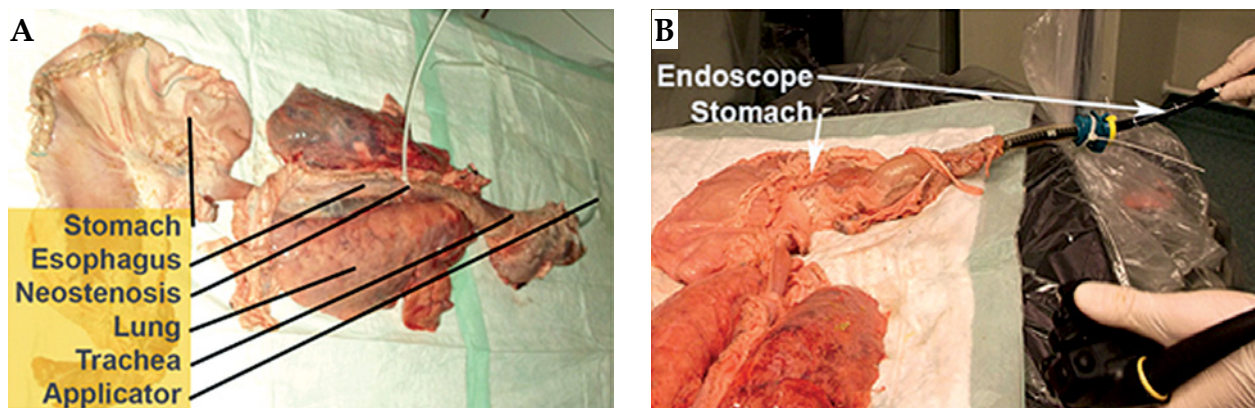

Fig. 9. Gamma evaluation outcomes

Fig. 10. A) Porcine respiratory and upper digestive anatomy; **B**) Endoscopy setup

during *ex vivo* experiments with porcine material. Preparation of the porcine material (Figure 10) took place in the endoscopy department. Stringent precautions were implemented at all study sites (endoscopy, CT scanning). Surfaces, including cabinets, were sealed with waterproof drapes, and mobile objects were removed (Figure 11). Only single-use or research-dedicated equipment was employed. All staff wore full personal protective equipment (PPE), including waterproof gowns, overshoes, surgical caps, face masks, and gloves, which were changed upon leaving the room. Strict hand hygiene protocols were followed after PPE removal.

Post-experiment, qualified staff performed thorough disinfection of all surfaces using a peracetic acid-based powder concentrate (Ultrasol® Active 1%, Corsair Pharma, Germany). Safety measures were adapted from hospital protocols for managing patients with multi-drug-resistant Gram-negative bacteria. The Department for Hygiene and Environmental Medicine supervised the adherence to safety measures throughout the study. All biomaterial, consumables, and materials in contact with porcine tissue were disposed of as biohazardous and potentially infectious waste. The applicator's feasibility was evaluated with an *ex vivo* porcine model simulating the upper gastrointestinal tract [22]. A porcine specimen, including the tongue, pharynx, esophagus, stomach, duodenum, lungs, and thoracic aorta, was obtained from a local butcher. It was transported at 4°C, frozen at –20°C, and then thawed to 4°C before the experiment.

The antrum of the stomach was incised, residual contents removed, and the incision was closed with surgical sutures. A gastroscope (GIF-1TH190, EVIS EXERA III, Olympus Medical, Tokyo, Japan) was inserted through the duodenum to inspect the esophageal mucosa for any
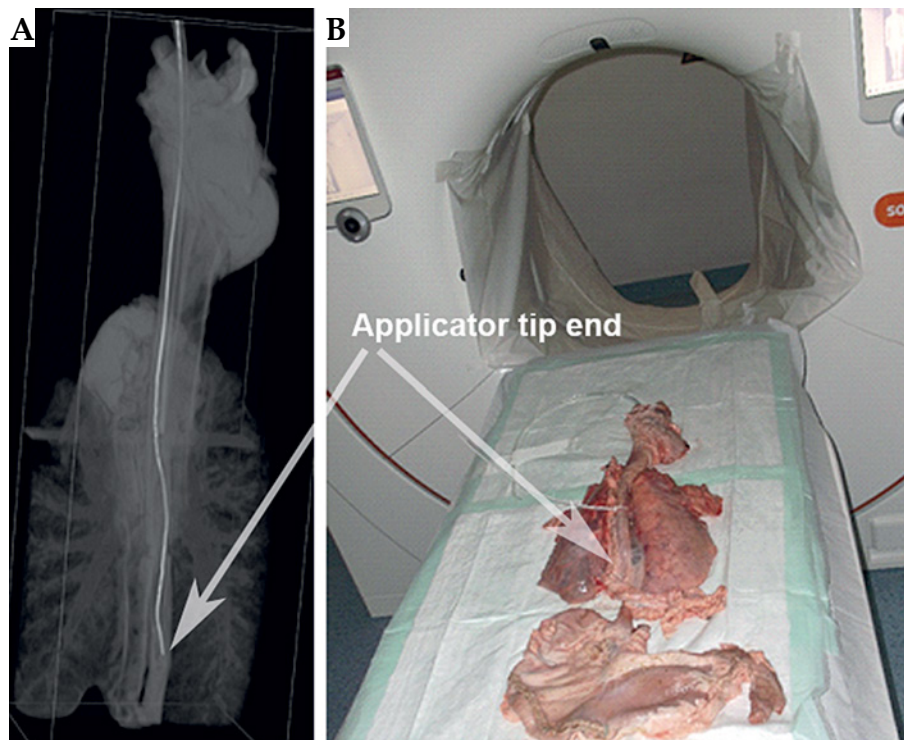

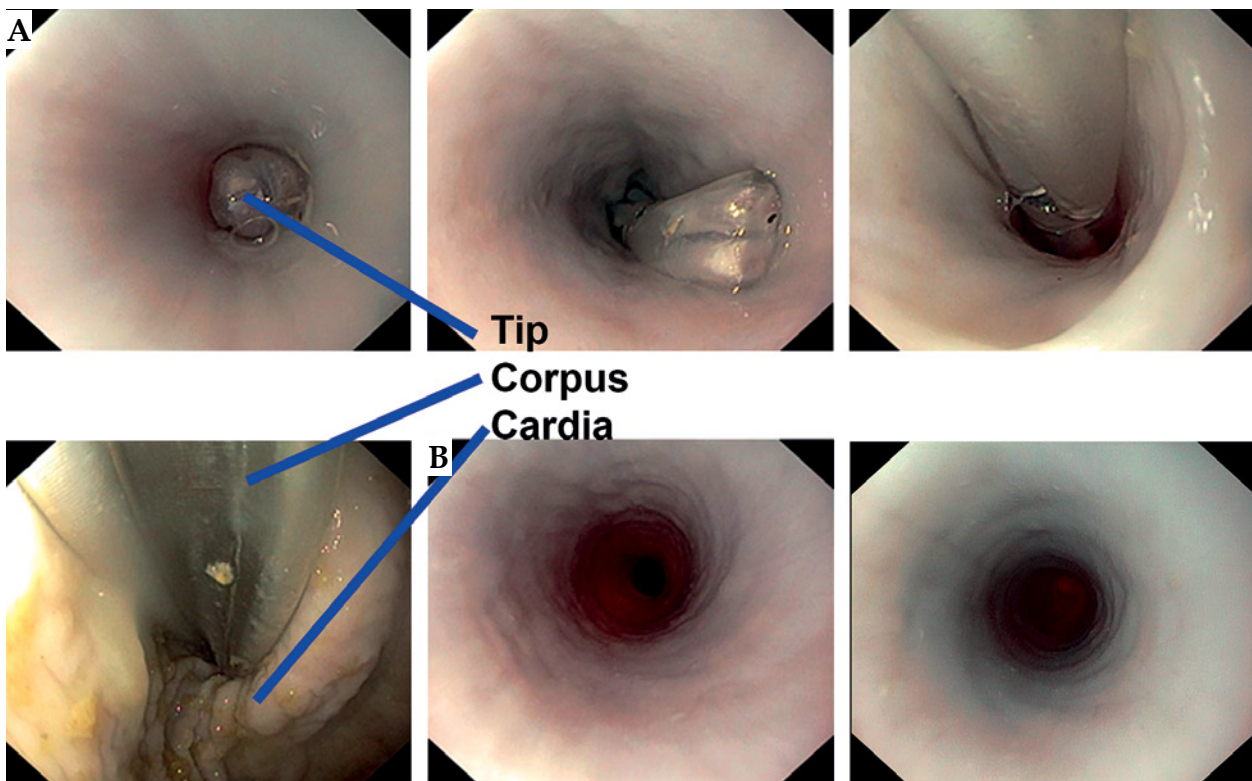**Fig. 11. A**) DDR of *ex vivo* porcine organs; **B**) CT setup

Fig. 12. A) Insertion of the applicator from the esophagus into the stomach; **B**) State of the esophagus after removal

pre-existing lesions. Subsequently, the applicator was introduced through the upper esophageal sphincter under endoscopic guidance and advanced into the stomach.

After removing the applicator, the esophagus underwent a second endoscopic inspection. Then, the applicator was re-introduced, and a neostenosis was created around its corpus using a zip tie to simulate a stenosis. The specimen was then analyzed using computed tomography for dose determination (Figure 11).

The applicator could be smoothly advanced into the stomach, and endoscopic surveillance showed no signs of trauma to the organ. Inspection after applicator removal showed no mucosal lesions in the esophagus (Figure 12). The zip tie effectively created a tight neostenosis of approximately 10 mm in diameter around the applicator corpus, successfully simulating a stenosis (Figure 13). The entire procedure, including endoscopy and CT scans, was completed within approximately 45 minutes, simulating an in-patient treatment scenario.

Discussion

The study effectively demonstrates feasibility of using 3D printing technology for the design of esophageal
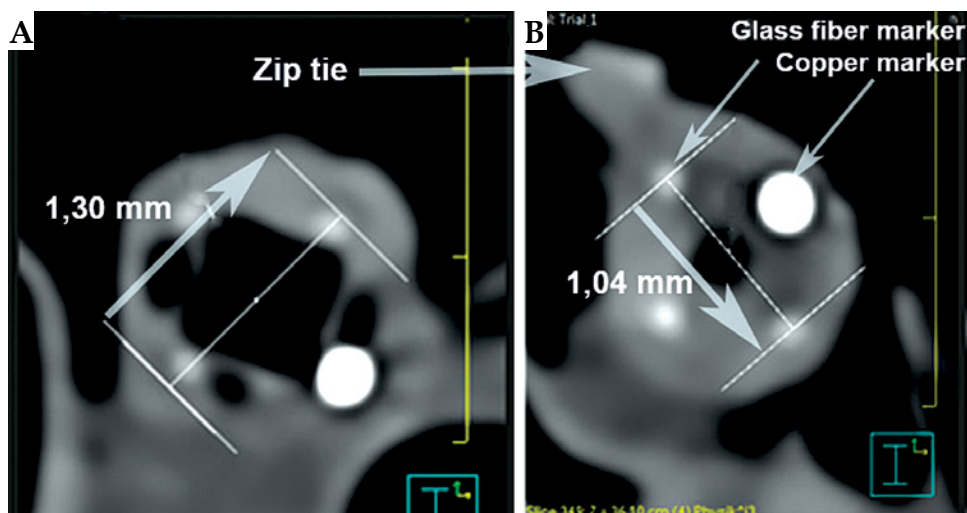

Fig. 13. CT images. **A**) Applicator before neostenosis; **B**) Applicator in neostenosis
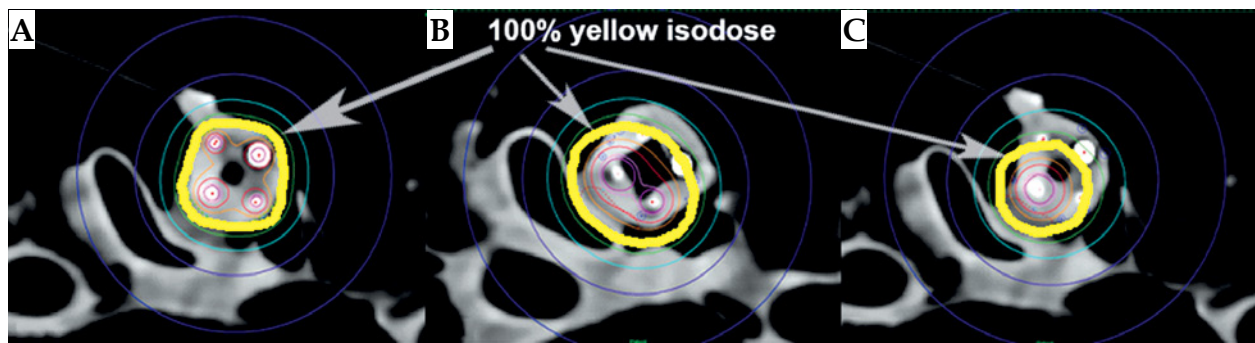
Fig. 14. Dose distribution comparison. **A**) 4 loaded channels, **B**) 2 loaded channels, and **C**) 1 loaded channel

brachytherapy applicator. The use of auxetic structures in the applicator design enhances its adaptability and structural integrity, which is crucial for accommodating varying internal body pressures during insertion procedures. Previously, this innovative approach has shown promising dosimetric outcomes, including improved dose delivery accuracy and enhanced tissue sparing, as evidenced by initial trials conducted on a porcine model (Figure 14). However, the limitation of these trials being non-human studies necessitates further validation in larger clinical cohorts to confirm efficacy and safety in human patients.

Economic analysis indicates that the novel applicator has the potential to be a cost-effective alternative to currently employed methods. The reduced costs associated with sterilization management and production, along with streamlined logistical operations, contribute to the economic viability of this solution. Furthermore, the single-use design facilitates the treatment of multiple patients consecutively, enhancing its practicality and suitability for clinical implementation. The successful integration of 3D printing technology within hospital settings is contingent upon the ability to keep pace with the rapid advancements in materials, expertise, and the evolving technological landscape, thus ensuring the effective adoption and utilization of this innovative approach [23].

From a radiotherapy perspective, the advantages of this applicator are expected to improve conformity with the endoluminal anatomy (stenosis, tumor) and more homogeneous coverage of the target volume. Additionally, the potential for the applicator to be used in various clinical applications and treatment modalities will be explored, particularly for disease sites requiring access through lumens smaller than 10 mm in diameter [24].

Although the selected biocompatible material offers tailor ability and precision in 3D printing, there is an ongoing need to explore materials, which also provide benefits of recyclability or biodegradability. This consideration is crucial for reducing the environmental impact of single-use medical devices and aligning with sustainability goals in medical manufacturing [25].

The primary limitation of the study is its reliance on non-human trials, which (while providing initial insights into the applicator's performance) do not fully replicate the complexities of human anatomy and disease pathology. Extensive clinical trials involving human subjects are essential to validate the findings, and ensure safety and ef-

fectiveness of the applicator in a clinical setting. Moreover, continuous adaptation and optimization of the applicator design is necessary to keep pace with advancements in 3D printing technology and patient care standards.

Conclusions

The development and implementation of the novel applicator are feasible, leading to a consistent and reliable distribution of the dose in *ex vivo* settings. The current findings indicate positive outcomes from *ex vivo* test, further supporting the efficacy of this approach. The applicator's potential for improving patient outcomes, reducing healthcare costs, and enhancing treatment conformability, make it an attractive option for the treatment of esophageal cancer.

Disclosures

Approval of the Bioethics Committee was not required.

The authors declare no conflict of interest.

References

1. Regulation (EU) 2017/745 of the European Parliament and of the Council on medical devices Date: April 5, 2017. https://eur-lex.europa.eu/legal-content/EN/TXT/?uri=celex-%3A32017R0745
2. Good Manufacturing Practice (GMP) Guidelines – Annex 1: Manufacture of Sterile Medicinal Products. [Guideline]. Au-

gust 25, 2022. Available from: https://health.ec.europa.eu/system/files/2022-08/20220825_gmp-an1_en_0.pdf

3. Council of the European Communities. Council Directive 93/42/EEC of 14 June 1993 concerning medical devices. Official Journal of the European Communities 1993; L 169: 1-43. Available from: https://eur-lex.europa.eu/legal-content/EN/TXT/?uri=celex%3A31993L0042

4. Robert Koch-Institut-Krebs in Deutschland 2023. Kapitel 15: Speiseröhre. Berlin 2023. Available from: https://www.krebsdaten.de/Krebs/DE/Content/Publikationen/Krebs_in_Deutschland/kid_2023/kid_2023_c15_speiseroehre.pdf

5. Mangesius J, Hörmandinger K, Jäger R et al. Chemoradiotherapy combined with brachytherapy for the definitive treatment of esophageal carcinoma. *Cancers (Basel)* 2023; 15: 3594.

6. Buzurovic IM, Hansen JL, Bhagwat MS et al. Clinical implementation of a novel applicator in high-dose-rate brachytherapy treatment of esophageal cancer. *J Contemp Brachytherapy* 2016; 8: 319-325.

7. Kulshrestha R, Gupta A, Sharma DN, et al. Brachytherapy for oesophageal carcinoma: A comprehensive review of literature and techniques. *J Radiother Pract* 2022; 21: 267-276.

8. Formlabs. Technical Data Sheet: BioMed Flex 80A. [Internet] (cited 2023). Available from: https://formlabs-media.formlabs.com/datasheets/TDS_-_BioMed_Flex_80A_-_Digital_A5.pdf

9. Grumezescu V, Grumezescu A. Materials for biomedical engineering: Thermoset and thermoplastic polymers. 1st ed. 2019. ISBN: 9780128168752.

10. Jigang H. A review of stereolithography: Processes and systems. Processes. 8. 1138. 10.3390/pr8091138. 2020. https://doi.org/10.3390/pr8091138

11. International Organization for Standardization. Rubber, Vulcanized or Thermoplastic – Determination of Indentation Hardness. Part 1: Durometer Method (Shore Hardness) (ISO 7619-1:2010). [Standard]. 2010.

12. Zeus Inc. Nylon 6-6 Material. [Internet] (cited 2023). Available from: https://www.zeusinc.com/wp-content/uploads/2023/09/Nylon-6-6-Material-V1R2.pdf

13. Feng H, Lv W, Ma J, et al. Helical structures with switchable and hierarchical chirality. *Appl Phys Lett* 2020; 116: 194102.

14. Park FC, Ravani B (1997). Smooth invariant interpolation of rotations. *ACM Transactions on Graphics* 1997; 16: 277–295.

15. Lim TC. Auxetic Materials and Structures. 2015. ISBN: 978-981-287-274-6.

16. Rouf S, Raina A, Haq MI et al. 3D printed parts and mechanical properties: Influencing parameters, sustainability aspects, global market scenario, challenges and applications. *Adv Ind Eng Polym Res* 2022; 5: 143-158.

17. Auricchio F, Bacigalupo A, Gambarotta L et al. A novel layered topology of auxetic materials based on the tetrachiral honeycomb microstructure. *Mater Des* 2019; 179: 107883.

18. Budynas RG, Nisbett JK. Shigley's mechanical engineering design. 9th ed. McGraw-Hill, New York 2011.

19. Zwierzchowski G, Bielęda G, Skowronek J et al. Film based verification of calculation algorithms used for brachytherapy planning-getting ready for upcoming challenges of MBDCA. *J Contemp Brachytherapy* 2016; 8: 326-335.

20. Pócza T, Zongor Z, Melles-Bencsik B et al. Comparison of three film analysis softwares using EBT2 and EBT3 films in radiotherapy. *Radiol Oncol* 2020; 54: 505-512.

21. Zhao A, Gao S, Greskovich J et al. Pre-clinical dosimetry of a new six-channel applicator for high-dose-rate treatment of esophageal cancer. *J Contemp Brachytherapy* 2021; 13: 318-324.

22. Parra-Blanco A, Gonzalez N, Arnau MR. Ex vivo and in vivo models for endoscopic submucosal dissection training. *Clin Endosc* 2012; 45: 350-357.

23. Thiveaud D, Durand F, Hajjar J et al. Costs of purchase, maintenance, microbiological control, and reprocessing of a reusable duodenoscope. *Endosc Int Open* 2023; 11: E873-E879.

24. Kinoshita Y, Furuta K, Adachi K et al. Asymmetrical circumferential distribution of esophagogastric junctional lesions: anatomical and physiological considerations. *J Gastroenterol* 2009; 44: 812-818.

25. Hellman S, Frisch P, Platzman A et al. 3D printing in a hospital: Centralized clinical implementation and applications for comprehensive care. *Digit Health* 2023; 9: 20552076231221899.